A new three-dimensional CFD model for efficiency optimisation of fluid-to-air multi-fin heat exchanger

Miftah Altwieb[1], Krzysztof J. Kubiak [2], Aliyu M. Aliyu[3], Rakesh Mishra [3]

[1]Department of Mechanical and Industrial Engineering, University of Gharyan, Libya
[2]School of Mechanical Engineering, University of Leeds, United Kingdom
[3]School of Computing and Engineering, University of Huddersfield, United Kingdom

Abstract

New simulation and experimental results have been obtained and are presented for a multi-tube fin heat exchanger unit, from which semi-analytical correlations for the Fanning friction and Colburn factors were developed. The multi-tube and fin heat exchanger represents the main component of the Fan Coil Unit, an essential component of HVAC systems used for domestic and commercial heating and cooling. Improving the efficiency of the heat exchanger typically comes at the expense of higher pressure drops or costlier materials and production costs. Here, an experimental setup was designed and constructed to evaluate the thermal performance of such a heat exchanger. Geometrical modifications were explored for thermal performance enhancement. Furthermore, full three-dimensional CFD case studies of the heat exchanger were investigated to examine the effect of the geometrical features on the air side of the heat exchanger to study the effect of fin spacing, transverse and longitudinal pitches. The CFD model developed was first globally validated against experimental results. The model results were used to predict the Fanning and Colburn factors and the local fin efficiency based on the carefully selected geometric parameters. The data obtained was utilised to develop two new semi-analytical models for the Fanning and Colburn friction factors which were well within ±10% error bands and showed strong correlation coefficients of more than 98 and 97% respectively.

Key Words: CFD modelling, Colburn factor, Fanning friction factor, fin efficiency, heat exchangers.

1   INTRODUCTION

There is an undoubted increase in global demand for heating and cooling of residential and industrial buildings. This in turn leads to a rapid increase in the CO_2 footprint due to commercial and domestic heating and cooling. Climate scientists have warned of the environmental impact of human activities fast approaching an irreversible point, that will create a permanent change to the planet's natural environment. Therefore, increasing the efficiency of Heating, Ventilation and Air Conditioning (HVAC) systems will undoubtedly have a significant impact on achieving net zero carbon goals set by governments around the world. For example, the UK government is aiming to achieve net zero carbon emission target by 2050 [1]. Improving the efficiency of energy systems including HVAC devices such as fan and coil units is key to achieving this target. A Fan Coil Unit (FCU) mainly consists of a heating or cooling coil and a fan. Normally, an FCU is coupled to the pipework for controlling the temperature in the installed space [2].

Cavallini et al. [3] reported work carried out on a HVAC system with smooth tubes where the behaviour of pure/blended halogenated and high-pressure hydrofluorocarbons (HFC) was studied. The heat transfer coefficient as well as the pressure drop characteristics during condensation were investigated. They proposed a new predicting model based on the flow patterns that occur during the condensation process. They showed that predictions from their model agreed with a large experimental data bank from the literature. While their work and others in the literature are important work, the awareness on climate change and global warming means that further research into more sustainable refrigerants for HVAC systems is needed.

For example, Mohammadshahi et al. [4] report an innovative use of the traditional Shavadoon HVAC system via a numerical study. It uses natural convection and their results showed that it has the ability to radically reduce the ambient temperature and maintain comfort conditions. They varied the system's geometrical parameters e.g. valve at the canal outlet, its location and diameter and concluded that using an S-shaped intake with an exit controlling valve improved the ventilation without deteriorating the thermal comfort conditions. Therefore, it can effectively decrease energy consumption and prevent possible environmental damage caused by conventional HVAC systems that use HFCs and other refrigerants that have been shown to have adverse effects on the environment.

Numerous studies have been carried out reporting various improvement schemes for the efficiency of FCUs and other heat exchanger systems in order to handle a certain heating or cooling duty. In general, techniques of augmentation or enhancement are divided into active, where external forces are employed to enhance heat transfer characteristics; and passive techniques, which use surface or geometric adjustments to the flow channel by using inserts or additional tools. Alternatively, combining passive and active methods can be used to further boost a heat exchanger's thermo-hydraulic performance [5].

Wang and Chi [6] examined the air-side efficiency of fine and tube heat exchangers with the configuration of a simple fin. Eighteen samples were studied to analyse the effect on thermal and flow characteristics of the number of fin spacing, number of tube rows, and the tube diameter. It was concluded that for a Reynolds number range i.e. $Re = 300–3000$, and for one and two tube rows, the fin pitch clearly influences the heat transfer behaviour. In addition, a very small influence of the number of rows was noticed on the friction performance and the influence of the tube diameter on the heat transfer output is related to the fin pitch, which was consistent with the results reported in their earlier study [7]. For a louvered fin-and-tube heat exchanger without louvre redirection, Wang et al. [8] experimentally found that that the friction factors are unaffected by the number of tube rows, more so at $Re > 2000$ and the heat transfer coefficients were found to significantly reduce at conditions of $Re < 2000$ in the case of the six-row coil heat exchanger they studied. Furthermore, they discovered that the maximum j factor values occur at lower Re values and this corresponds to lower fin spacing and vortex formation; and that fin pitch does not affect the characteristics of heat transfer at $Re > 2000$. However, heat transfer coefficients are directly proportional to fin pitch. They finally derived a correlation for the Colburn and Fanning factors that described the data to with a 10% error band.

An experimental investigation of a compact heat exchanger unit was carried out by Shinde and Lin [9]. The fins were fitted with louvers and flat tubes and the air-side Re range was 20–200. Experiments were carried out with twenty-six different corrugated louvered-fin heat exchangers. The data collected was used to derive correlations for the j and f factors in two Reynolds number ranges namely $Re = 20–80$ and $Re = 80–200$. They concluded that airflow and heat transfer characteristics are different at very low and high Reynolds numbers. It is noted that their Reynolds number range is rather narrow and cannot be applied for applications with requirements of high flow throughput.
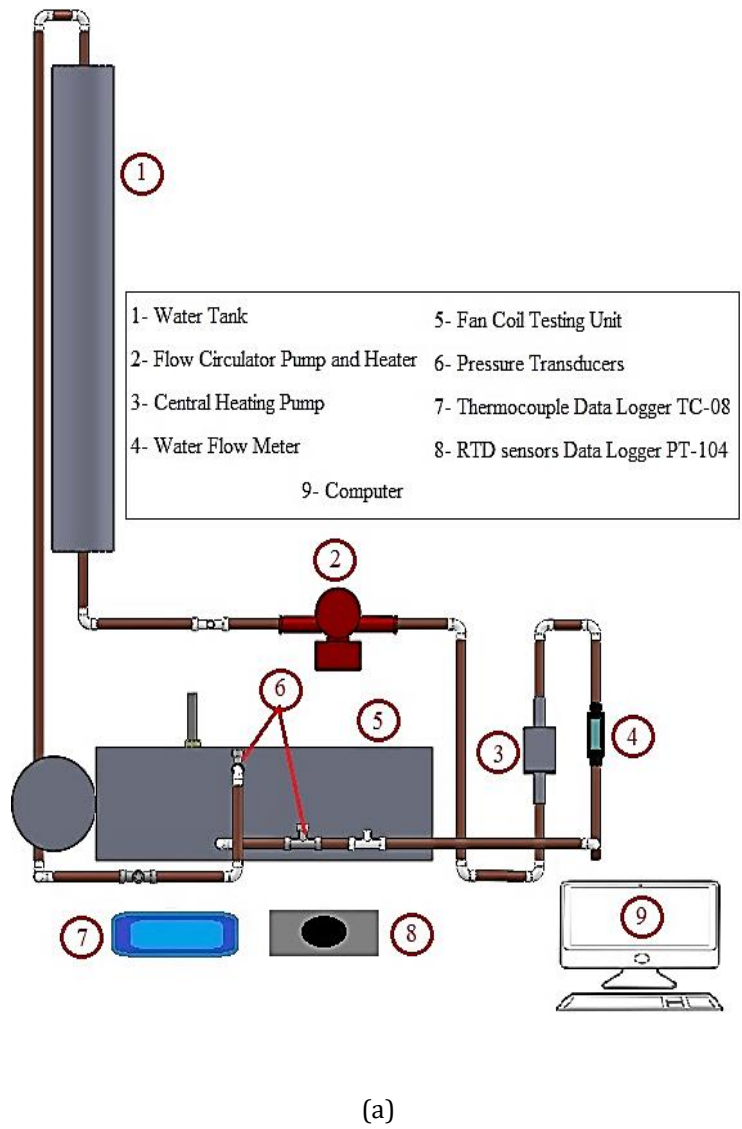
Taler [10] proposed two methods for calculating the coefficient heat transfer on the air side for a two-pass radiator consisting of two aligned rows of oval-shaped tubes having flat, simple fins. They obtained a correlation for the air-side heat transfer coefficient using experimental data. In addition, they inferred that the heat transfer coefficients are greater based on the difference in air temperature through the heat exchanger determined using the latter approach i.e. computational fluid dynamics (CFD). This is because their CFD model does not consider conductance caused by the thermal interaction between the pipes and fins. Dong et al. [11] reported an experimental and CFD study of pressure loss and thermal performance for airflow through a wavy fin in the fully-developed

turbulent regime. The wavy fin profiles they used are: triangular round corner, sinusoidal and triangular. Findings of this investigation suggested the wavy fin profiles had almost no effect on f and heat transfer efficiency. They also stated that the standard $k - \varepsilon$ turbulence model was the most appropriate for simulating air flow and heat transfer of their wavy fin configurations for the range of $Re = 1000$ to 5500.
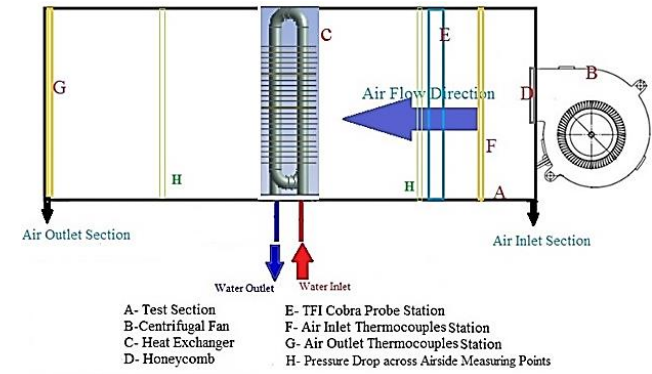
While experimental studies are most desirable, there can be huge costs involved in setting them up especially if several configurations are to be examined. As a result, numerical research on fin and tube heat exchangers has recently been done using CFD. It is noted that the reported works have a rather restricted range of factors examined with most CFD studies using a computational framework that takes only part of the fin into account. Furthermore, most of these studies neglect local flow distribution analysis, such as those of temperature, heat transfer coefficient, as well as the local fin efficiency of working fluids and fins. Identifying the improvement of these local flow characteristics can improve the efficiency of the heat exchanger.

Lu et al. [12] investigated the geometrical features on the performance of a fin-and-tube heat exchanger with six tube rows for refrigerator applications. They studied the effects of tube pitch, its diameter, fin pitch, and their thickness. They measured the heat exchanger performance in terms of the ratio of heat transfer rate to pressure drop as well as the coefficient of performance. It was found that performance increased with longitudinal and transverse tube pitch, but it decreased with tube diameter and fin thickness. However, the study was carried out on a partial heat exchanger geometry, and the effect of the different geometrical parameters cannot be confidently extrapolated to model the behaviour of the full heat exchanger geometry. The same can be said for the study of Lin et al. [13] where they reported a CFD investigation over a staggered circular tube bank fin heat exchanger with an interrupted half annular groove fin. They observed that at lower Reynolds numbers, the fin surface did not significantly affect heat transfer but much better performance was achieved at higher Reynolds numbers. There was a mean increase of 10–40% in the f factor and Nusselt number of the annular groove fin was obtained in comparison to that of the baseline plain fin with heat transfer performance increasing 7.0% to 27.0% when Re increased from 600 to 2500 respectively. Again, their work was on part of the heat exchanger geometry and little or no information can be inferred for the full thermal characteristics of the heat exchanger.

In a CFD study, Čarija et al. [14] analysed air-side flow of a fin and tube heat exchanger having multiple rows with flat and louvered. An Re range of 70–350, calculated using fin spacing and front air velocities, was used. They showed that there was improved heat transfer performance of nearly 60% for the louvered fins at $Re = 350$ in comparison to flat fins. Additionally, as the length of the louvre increases, the heat transfer efficiency proportionally increased for the same Reynolds numbers. Altwieb et al. [15] performed a CFD study with benchmarking experiments to measure performance characteristics of a multi-tube and fin heat exchanger at steady state. A three-dimensional computational model with complete heat exchanger geometry was developed. They explored the performance of several fin configurations: louvered, semi-dimpled vortex generator, and plain. The results showed that the thin vortex generator fins produced the highest non-dimensional heat transfer parameter hence best performance of the fin configurations studied. Two dimensionless empirical equations were derived from the simulation data. They suggested that the relationships can be used for sizing and design of the heat exchangers to estimate the rate of heat transfer and the pressure characteristics on the air side.

1- Water Tank
5- Fan Coil Testing Unit

2- Flow Circulator Pump and Heater
6- Pressure Transducers

3- Central Heating Pump
7- Thermocouple Data Logger TC-08

4- Water Flow Meter
8- RTD sensors Data Logger PT-104

9- Computer

(a)

Air Flow Direction

Air Outlet Section

Air Inlet Section

Water Outlet   Water Inlet

A- Test Section
E- TFI Cobra Probe Station
B-Centrifugal Fan
F- Air Inlet Thermocouples Station
C- Heat Exchanger
G- Air Outlet Thermocouples Station
D- Honeycomb
H- Pressure Drop across Airside Measuring Points

(b)
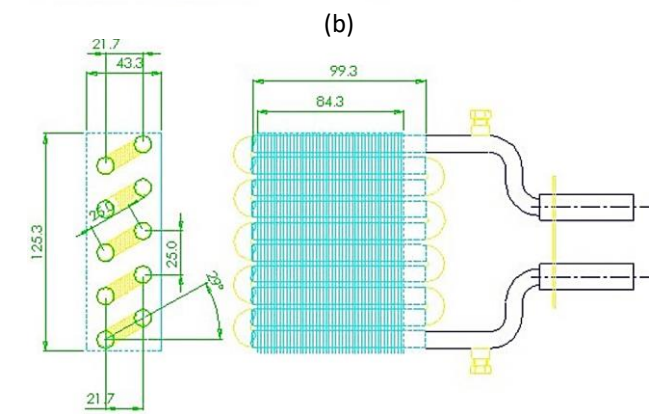
(c)
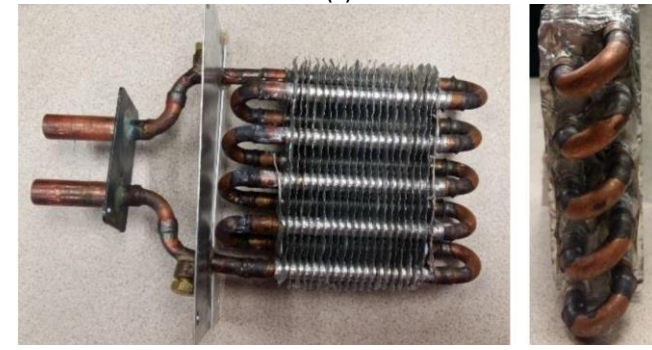
(d)

Figure 1: Schematic showing (a) overall experiment Setup (b) heat Exchanger testing unit (c) heat exchanger dimensions (in mm) (d) image of fin heat exchanger

The current investigation presents a qualitative as well as quantitative evaluation of a full-geometry fin and multi-tube heat exchanger having plain fins. A number of numerical simulations were carried out which were well-validated with experimental measurements. The analysis carried out is important for understanding the complex flow behaviour of the heat exchanger with plain fins. In addition, a parametric analysis of geometric features on pressure drop and heat transfer attributes of the heat exchanger represented by the friction and Colburn factors. We consider steady state conditions. The data from this study has been used to establish a new set of semi-empirical correlations that consider the effects of geometric parameters and can be used for the optimisation of heat exchanger efficiency.

2   EXPERIMENTS

2.1   Experimental Setup

Planning and conducting experiments are an important step in studying the thermal and hydraulic performance of heat exchanges as they provide vital measurements for the validation of simulation results. Figure 1 (a) shows the complete experimental setup used to obtain temperature and pressure differences across the current heat exchanger system at different inlet flow conditions. It comprises of a water tank, a pump, flow meter, a heat exchanger testing unit, pressure transducers, a data logger for thermocouples, a data logger for RTD temperature sensors and a windows-based personal computer. There are a variety of fin types, such as plain, louvered, convex-louvered, and wavy. Among these designs, the most common fin design in heat exchanger applications is the simple fin configuration, due to its simplicity and rigidity, and has been used in this work. Furthermore, circular tubes are common geometries used in such heat exchangers [5]. An experimental setup was conceptualised, designed and constructed to conduct steady-state experiments on a multi-tube and fin heat exchanger. Figure 1 (b) presents the schematic diagram of the heat exchanger test unit. The test unit was manufactured using a 2 mm thick galvanised steel sheet. The test section's length is 650 mm, a width of 165 mm and height of 175 mm. It consists mainly of a one-sided centrifugal fan having an integrated electronically-commutated (EC) motor to drive the ambient air flow through the test unit, the heat exchanger and the following measuring components.:

- TFI Cobra Probes for air velocity measurement
- Temperature of the inlet and outlet air measurement stations, each of which consists of T-type exposed welded tip thermocouples made of a Copper–Constantan alloy [6], [16] for the study of temperature distribution (7 in number)
- Micro-Manometer for the measurement of air-side pressure drop
- Flow Straightener (Honeycomb Structure) for turbulence suppression at the air inlet

The heat exchanger system utilised consists of two rows of tubes with a diameter of 9,52 mm, each row comprises 5 tubes, with the length of each tube being 130 mm and connected with a bend of 16 mm. Tubes are made of copper with a thickness of 0.26 mm. The heat exchanger consists of twenty-one staggered plain aluminium fins with a thickness of 0.12 mm. The fins are 43.3 mm apart and 125.3 mm in height. The fins are spaced 4.23 mm apart (6 fins per inch). Figure 1 (c) shows the detailed dimensions of the heat exchanger.

2.2   Experimental tests Procedure

Steady state experiments are the simplest type of experiments to conduct and analyse as the flow is time independent. In the present analysis, experiments were carried out by drawing flow of air through the fins of the heat exchanger while hot water was flowing in the heat exchanger tubes. The air velocity used here is within a range of 0.7–5 m/sec, representing the mean velocity of the airflow across the square duct measured using ASHRAE 41.2 standard [17] and widely reported [18],

[19]. The temperature of the air inlet is 24 ± 1 °C. The water flow rate range is between 2.0 L/min and 6.0 L/min. Inlet and outlet temperatures were determined by Pico resistance temperature detector probes (model RTD-PT100) [16]. The temperature of the inlet water was kept constant at 60.0 ± 1 °C.

2.3   Data Analysis

The temperatures at both air and water inlets; and air and water outlets were measured along with the pressure drop across the water and the air sides. For the heat transfer rate, the effectiveness–number of transfer units (or ε-NTU) method is used. This method is mostly for counter-current heat exchangers in preference to the log-mean temperature difference (LMTD) method in cases where there is inadequate information for the calculation of the LMTD. The number of heat transfer units (NTU) is computed as follows:

$$NTU = UA/C_{\min} \tag{1}$$

where $C_{min} = m_{min}c_{p,min}$ with m_{min} and $c_{p,min}$ being the mass and specific heat capacity of the fluid with the lower heat capacity rate (the air side in this case). The air and water side heat transfer are expressed as:

$$\dot{Q}_w = \dot{m}_w Cp_w(T_{wi} - T_{wo}) \tag{2}$$

$$\dot{Q}_a = \dot{m}_a Cp_a(T_{ao} - T_{ai}) \tag{3}$$

In order to minimise any drop in j, data reduction based on the mean rate of heat transfer $\dot{Q}_{avg}$ is done [20]. Therefore, $\dot{Q}_{avg}$ can be calculated as follows:

$$\dot{Q}_{avg} = \frac{\dot{Q}_w + \dot{Q}_a}{2} \tag{4}$$

The heat exchanger effectiveness (ε) is the ratio of the actual to the maximum achievable heat transfer rate. As a result, a relationship for ε can be written as:

$$\varepsilon = \frac{\dot{Q}_{avg}}{C_{min}(T_{wi} - T_{ai})} \tag{5}$$

The maximum achievable heat transfer rate is obtained when the temperature difference between the inlet and outlet streams is at a maximum. The quantity UA, also known as the overall conductance, is given by [15]:

$$UA = \frac{1}{\dfrac{1}{\eta_o h_a A_a} + R_{wall} + \dfrac{1}{h_w A_w}} \tag{6}$$

where h_w and h_a are the water and air heat transfer coefficients respectively; A_w and A_a are the heat transfer areas for the water and the air surfaces respectively; and R_{wall} is the thermal resistance of the wall. Where a flat wall is involved, the thermal resistance is given as:

$$R_{wall} = \frac{\delta_{wall}}{k_{wall}A_{wall}} \tag{7}$$

where δ_{wall} is the thickness of the wall, k_{wall} is the wall material's thermal conductivity; A_{wall} is the wall heat transfer area; and the heat transfer coefficient of the water-side h_w is calculated using the Gnielinski [21] correlation:

$$h_w = \left(\frac{k}{D}\right)_w \frac{(Re_{D_w} - 1000)P_r \left(f_i/2\right)}{1 + 12.7\sqrt{\left(f_i/2\right)\left(P_r^{2/3} - 1\right)}} \tag{8}$$

Where f_i is the water–wall friction factor, and it is given by:

$$f_i = \left[1.58\, ln\left(Re_{D_w}\right) - 3.28\right]^{-2} \tag{9}$$

The Colburn j and Fanning f factors are calculated from Equations (10) and (11):

$$j = \frac{h_a}{\rho_a V_{a(max)} C_{pa}} \mathrm{Pr}^{2/3} \tag{10}$$

$$f = \frac{A_c}{A_o}\frac{\rho_m}{\rho_1}\left[\frac{2\rho_1 \Delta P}{G_c^2} - (K_i + 1 - \sigma^2) + (1 - \sigma^2 - K_e)\frac{\rho_1}{\rho_2} - 2\left(\frac{\rho_1}{\rho_2} - 1\right)\right] \tag{11}$$

Equation (11) was derived by Kays and London [22]. Where K_I and K_e are the sudden contraction and expansion pressure loss coefficients respectively, ρ_1 and ρ_2, and ρ_m are the air inlet, outlet, and mean air densities respectively; and σ is the ratio of the smallest flow area to the front area of the air duct.

3   NUMERICAL SIMULATION MODEL AND NUMERICAL METHODS

3.1   Numerical Simulation Model

Numerical simulations of heat exchanger configurations in this study were performed with the commercial software code ANSYS FLUENT 17.0 in order to determine the relationship between the configurations and performance. This was achieved in three stages namely pre-processing, the solver set up and the post-processing stage [23]. In the pre-processing stage, the geometry of the heat exchanger and flow domain were created and meshed in Design Modeller and ANSYS Meshing respectively. These were then imported into FLUENT in order to define the among other things the material properties, the boundary conditions, select the turbulence model, solution methods, and convergence criteria. Good theoretical and background knowledge is needed for a particular system in order to select the correct settings [24]which include spatial and temporal discretisation methods, the latter in the case of transient simulations. In the present work, time discretisation was not considered since steady simulations were carried out. The final stage of the modelling process is post-processing where the data are extracted at appropriate planes and results visualised [25].

Within this section, a novel CFD model including the complete 3D geometry of a single fin heat exchanger is presented. The heat exchanger design was developed using the commercial ANSYS Design Modeler software, and is shown in Figure 2. The model was made with the same geometry and dimensions as the experimental model consisting of 21 fins (4.23 mm apart) and made of aluminium with each fin having a thickness of 0.12 mm (6 fins per 2.54 mm). The fin was mounted in a computational domain (of dimensions 65 x 175 x 650 mm), which was divided into three parts (of dimensions 165 x 175 x 180, 165 x 175 x 60 and 165 x 175 x 410 mm) to help control the mesh size across the complex geometry of the heat exchanger tubes and fins.

The three-dimensional mass conservation (continuity), momentum and energy equations were simultaneously solved for the flow and temperature fields. The turbulent flow regime is considered by reference to the spectrum of experimental Reynolds numbers. The double precision steady-state solver and the SST $k-\omega$ turbulence model [26] were used primarily because it maintains the characteristics of the $k-\omega$ model near the wall and slowly decreases away from the wall to provide more accurate results [27]. The pressure, density, body force, the energy and momentum under-

relaxation factors used were respectively 0.3, 1.0, 1.0 and 0.7. The 2nd-order upwind discrimination scheme was used because it gives more accurate results [20] due to the truncation of the Taylor series to the 2nd term as against to the 1st in first order schemes. Gravitational acceleration was activated in the minus y-direction. Coupling of interfaces was done. ANSYS FLUENT enables two different walls to be combined, allowing the solver to compute quantities right from the solution in adjacent cells [23].
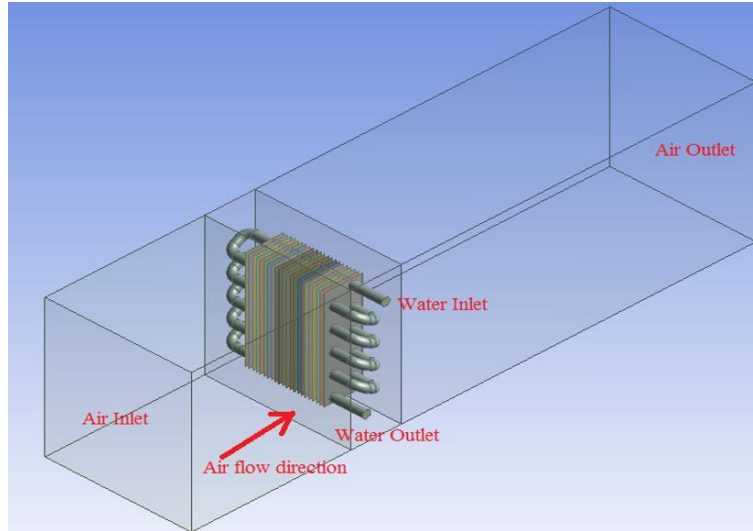

Figure 2: CFD Model for Multi-tube and Fin Heat Exchanger with Plain Fins

According to the ANSYS FLUENT user guide, the command' rpsetvar' (i.e.' temperature / secondary gradient? #f') should be added to turn off the secondary gradient to aid convergence in areas of low mesh quality [23] which can be done in regions of highly complex geometry such as those near tube curvature and between fins. The heat is transmitted through the walls by conduction. The thermal conductivity of the copper tubes was set at 387.6 W/m.K and the thermal conductivity of the aluminium fins was set at 202.4 W/m.K. The air and water properties used are as follows: densities $\rho_{water} = 998.2$ kg/m³, $\rho_{air} = 1.24$ kg/m³ (set as an incompressible ideal gas [23]); viscosities $\mu_{water} = 0.000471$ kg/m.s, $\mu_{air} = 0.00001789$ kg/m.s; and specific heat capacities $C_{p_{water}} = 4179$ J/kg.K, $C_{p_{air}} = 1005.684$ J/kg.K.
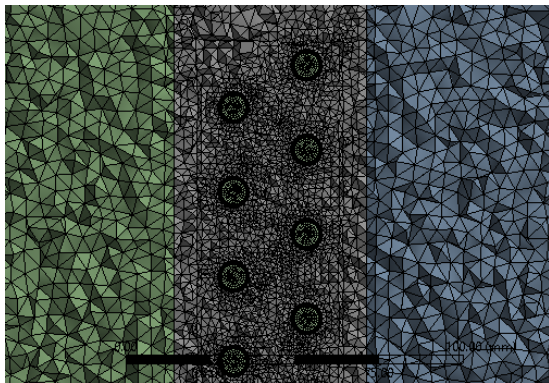
3.2   Meshing and Mesh Independence Test

A hybrid meshing technique [23] was adopted for the flow domain using tetrahedral (tetra) and quadrilateral (quad) mesh elements for the test section which was divided into three parts. The division splits the flow domain into the near field of the heat exchanger sandwiched between the air inlet and outlet sections. This allows for refining of the mesh to be carried out in the middle section to give finer mesh elements in the vicinity of the heat exchanger unit. Figure 3 (a) depicts the mesh density on the external surface of the computational domain. In order to generate quad mesh elements within the critical inflation layer region, a sweep method was adopted. Five inflation layers were added in the inner domain of the tubes, as well as adding a face sizing on the outer surface to enable finer meshes are obtained in the outer domain within the vicinity of the tubes. The SST $k-\omega$ turbulence model requires a near-wall spatial resolution where the value of y⁺ < 0.2 and a minimum value of y⁺ < 2 is required. As the present study focuses on the calculation of heat transfer, the automatic wall treatment in the $k-\omega$ model allows the consistent refining of the coarse and insensitive y⁺ mesh. It is therefore recommended to use a mesh with y⁺ about 1 [28]. Similar works in the literature have used the same turbulence model and showed its computational efficiency [26], [29]. This is because, The SST k-omega turbulence model has the ability to capture adverse velocity gradients and separated flows [30] which can develop in the downstream of the
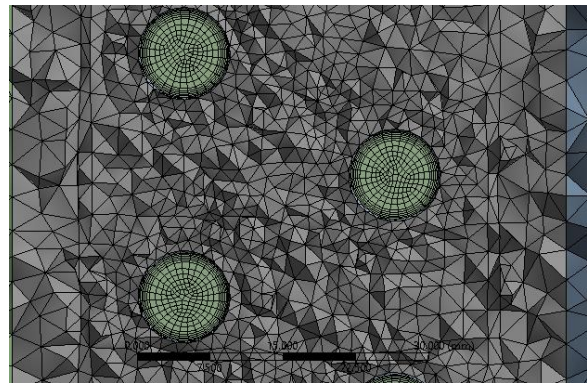
==flow around the tubes.== A mesh independence study was performed with three separate meshes. Meshes with 4, 8 and 12 million elements were selected for this study. In addition, the temperature of the air outlet was chosen as the parameter to compare the independency results, as it reflects the main results of the CFD modelling, indicating the system's performance.
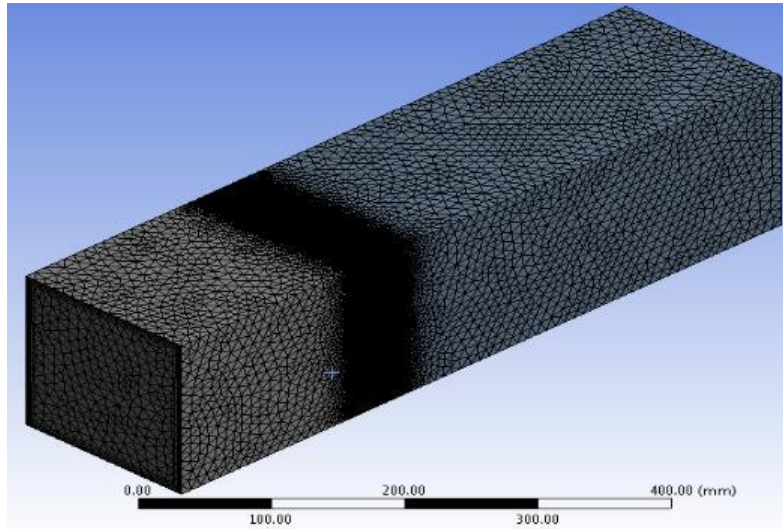
(a)

(b)

(c)

Figure 3: Model meshing showing (a) finer mesh elements around the heat exchanger ==(b) mid cross-section showing details of mesh around tubes and (c) details of inflation layers inside the tubes.==

Results of the mesh independency test are as given in Table 1. The mesh independency study shows a 4.9% difference in the temperature of the air outlet when the mesh elements were varied between 4 million and 8 million, while a 0.6% difference in temperature was obtained when number of mesh elements were increased from 8 million to 12 million. It was hence determined that the 8 million mesh elements model will provide enough accuracy, in good time and with a reasonable model size.

Table 1: Mesh Independence Test Results

Mesh size (millions)	Temperature of air outlet by CFD (° C)	Computation Time (h)	Absolute % difference	Time Saving (h)
4.0	31.39	4.5	---	---
8.0	32.92	8.6	4.9	4.1
12.0	33.11	11.7	0.6	3.1

3.3   Benchmark Tests

In numerical studies, the validation of mathematical method and models is immensely important in providing confidence in the simulation results. Validation or benchmarking involves conducting experimentation in a controlled laboratory-based environment with identical settings as in the

numerical model and evaluating the global performance indicators of the unit under test [31] and comparing with the numerical results. Minimal difference between the two at most or all of the input conditions tested is desired. Consequently, the numerical model can be considered to be well-validated, and confidence can be exercised on its results.

In this section, validation is provided for the CFD results the model includes a complete 3D heat exchanger geometry, and it was globally validated against the experimental water and air outlet pressure drops and temperatures on both the water and the air sides under different operating conditions. The variables represent the key outputs of the CFD model. They were plotted at the same water flow rate of 3.0 L/min and a mean air velocity of 2.2 m/s using identical boundary conditions as defined in section 2.3. Figure 4 (a) indicates a comparison of the numerical results and the experimental data for the heat exchanger water outlet temperature. It shows that the difference obtained between the CFD results and the water and air outlet temperatures from the experiments were quite minimal (<5% for the water outlet and the air outlet temperatures in all conditions measured and approximately 1% for the temperature of the water outlet). The pressure drop across the water side of the heat exchanger was measured by two pressure transducers (IMP - Industrial Pressure Transmitter). One was installed in the water inlet section while the other was in the outlet. The transducers were of a 3-wire, voltage output design with a range of 0 to 4 barg and nominal accuracy of ±0.25% of full scale. Therefore, the numerical data obtained from the results are considered to closely agree with the experimental measurements obtained for the full-geometry heat exchanger.

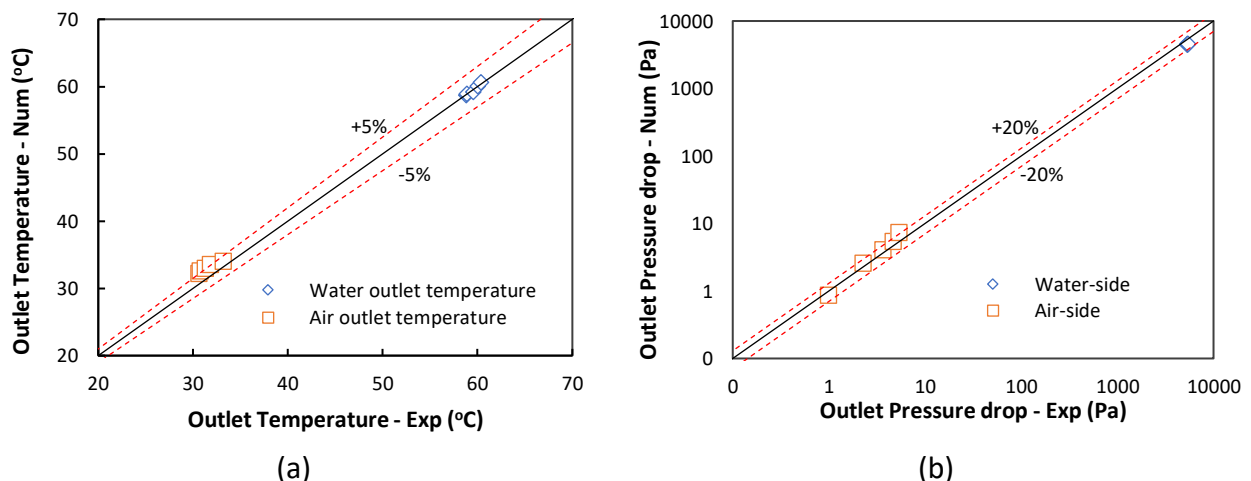(a)   (b)

Figure 4: A comparative validation between numerical (Num) and experimental (Exp) values for (a) outlet water and air temperatures and (b) air-side and the water-side pressure drops for the heat exchanger.

Figure 4 (b) illustrates a comparison of the numerical results and those of the experiments for the heat exchanger pressure drops at the water- and air-sides. These reveal that a good agreement was obtained between the CFD and experimental results for the water and air-side pressure drops. Due to the variability in the air- and water-side values, the pressure drop comparison was plotted on a log-log scale graph. The points for the water-side pressure drops range between 4,471 and 4,595 (four in number) and can be seen to cluster at the top right-hand corner of the plot. For all the points considered for the comparison, the percentage differences are observed to be less than 20%. Summarily, as a result of the benchmark experiments carried out in this section, it may be inferred that the CFD model we presented which included a full three-dimensional heat exchanger geometry is reliable. It was hence used to determine the pressure drop and heat transfer characteristics of the heat exchanger having plain fins at varying operating conditions with sufficient accuracy.

4   RESULTS AND DISCUSSION

4.1   Experimental Results

The results of the steady-state experiments carried out are presented in the form of plots of the Fanning f friction factor, the Colburn j factor and the efficiency index i.e. j/f with the water side Reynolds number ($Re_D \equiv \rho_{water} v_{water} D_{tube}/\mu_{water}$ with the quantities representing the water density, velocity, hydraulic diameter of the tube, and water viscosity respectively). Figure 5 presents the variations of j, f, and j/f with Re_D respectively. The computed values of j, f and j/f depending on the fluctuations of the input variables i.e. the inlet air and temperatures, the air velocity and water flow rate and have been shown in the calculation method in section 2.4. Hence, error bars have been included on the plots of j, f and j/f given in Figure 5 to quantify the fluctuations in these variables. As shown in Figure 5 (a), both the Colburn and the Fanning friction factors decline with an increase in the Reynolds number at a similar rate with the friction factor values much higher than the Colburn factors. As such, it is seen that at identical Reynolds number values, f is approximately three times the magnitude of j. However, the rate of decrease in j is higher than that of j. Similarly, j/f is plotted and presented in Figure 5 (b) and has an inverse relationship with Re_D trend as j and f.
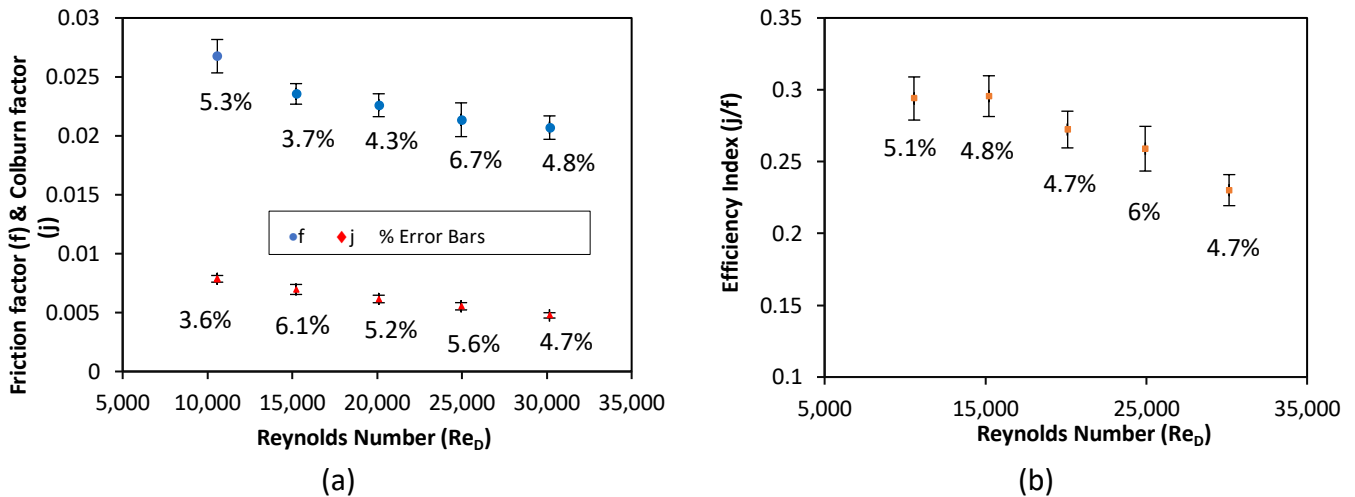

(a)   (b)

Figure 5: (a) Variations of (a) Colburn factor j and Fanning Friction Factor f (b) efficiency Index j/f with Reynolds Number (Re_D)

4.2   Determination of heat transfer coefficient and local fin efficiency prediction from CFD model results

The main aim of using fins is to maximize surface area and thus increase the overall rate of heat transfer. Heat passes through the fins by two methods namely conduction via the fins and convection from fin surface to air. The geometry, spatial arrangement and spacing of the fins has been shown to significantly affect the thermal efficiency of the heat exchanger unit [32].
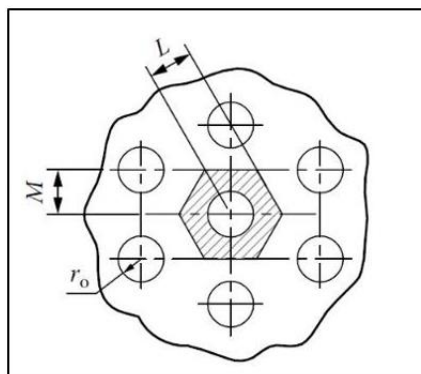

Figure 6: Geometry of the staggered fin arrangement [12]

Fins with dimples, holes or grooves or those with a corrugated or wavy geometry have been shown to generate different vortex patterns in the airflow than plain fins [33], [34]. For this reason, careful and accurate modelling is required for the prediction of heat transfer characteristics of any heat exchanger since to capture the effect of geometry on the fin efficiency which is a key parameter influencing air-side heat transfer [35]. Fin efficiency (η_f) is defined as the ratio of the actual heat transfer via the fin to the ideal (or theoretical) case where the entire fin is at the baseline temperature [19]. To determine fin efficiency of the heat exchanger, Schmidt's empirical method [36] was used.

Based on this method, and considering the geometrical configuration given in Figure 6, the fin efficiency was calculated [19], [37] using:

$$\eta_f = \frac{tanh(mr_o\phi)}{(mr_o\phi)}$$

(12)

where m is defined as,

$$m = \sqrt{\frac{2\,h_a}{k_a f_t}}$$

(13)

The variable h_a = fin air-side heat transfer coefficient (in W /m² K) which is obtained as a result from the CFD model; k_a is the fin material's thermal conductivity (in W/m K); f_t is the fin thickness; and r_o is the external tube radius. The variable ϕ is given as:

$$\phi = \left(\frac{R}{r_o} - 1\right)\left[1 + 0.35\,ln\left(R/r_o\right)\right]$$

(14)

where R is the radius of an equivalent circular fin having an identical efficiency as the rectangular fin. The ratio R/r_o for a staggered hexagonal tube bundle, it is shown in Figure 6 can be calculated as follows:

$$\frac{R}{r_o} = 1.27\psi\sqrt{\beta - 0.3}$$

(15)

where, $\psi = M/r_o$ and $\beta = L/M$. **Figure** 7 (a) and (b) give the results of these calculations for the local heat transfer coefficient and the fin efficiency for each fin respectively. These indicate that heat transfer coefficient as well as the fin efficiency vary locally depending on the prevailing flow conditions. The fins with the highest heat transfer coefficients are the least efficient. This is obviously the case when external fins 1 and 21 are considered. The heat transfer coefficients with the largest magnitudes were obtained at these fin locations (98.115 and 98.329 W/m²-K) and the lowest average efficiency was 0.748 and 0.749, respectively.
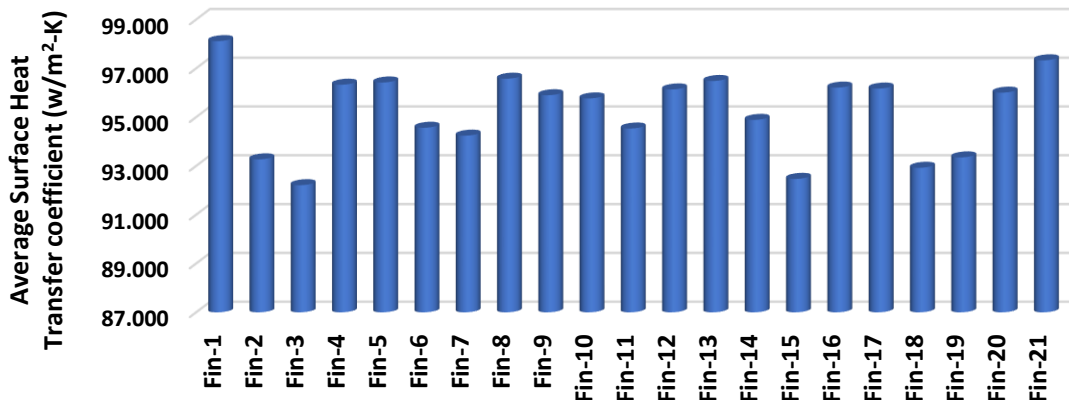
(a)
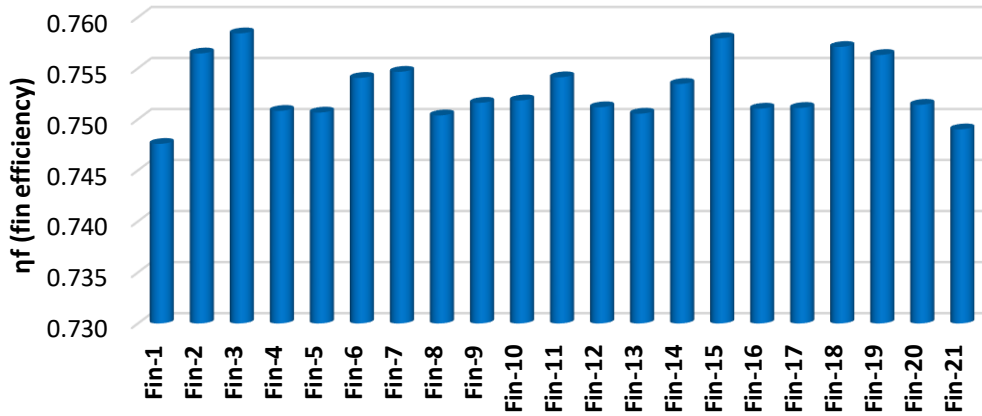
(b)

Figure 7: Local (a) heat transfer coefficient (b) fin efficiency for each fin in the heat exchanger calculated from the CFD simulation

Figure 8 displays contours of static temperature of the heat exchanger along with the local magnitudes of the air heat transfer coefficient. The magnitudes of the local fin capacity of the fins number 1, 5, 9, 13, 17 and 21. The figure indicates that the temperature distribution is different for each fin. In addition, the local magnitudes off fin efficiency and heat transfer coefficient of fins 5, 9, 13 and 17 are within a similar range due to differences in thermal characteristics of the heat exchanger fins, the condition in a fin should not be generalised to others, and thus it is imperative to evaluate the entire heat exchanger under this condition. This theory is consistent with the concept presented by Shah and London [38], where it was observed that the coefficient of heat transfer is not constant across its flow path but varies depending on factors such as position, entry-length effects (due to developing boundary layers), external temperature, the physical properties of the fluid, fouling, and manufacturing imperfections.
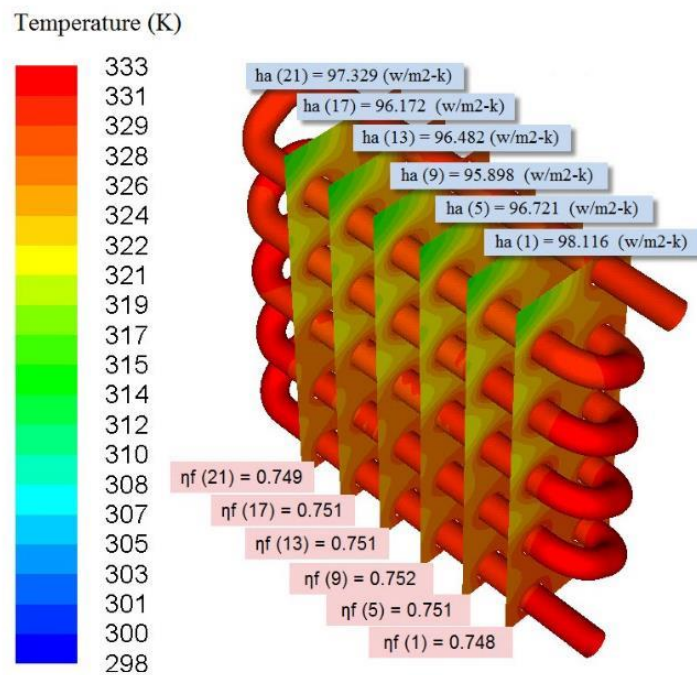

Figure 8: Static temperature contour for selected fins in the heat exchanger

4.3 Numerical comparison of air-side performance

The heat exchanger was numerically analysed to investigate the influence of fin spacing (F_p), longitudinal pitch (L_p) and transverse pitch (T_p) on the pressure gradient and heat transfer behaviour in steady state conditions. In this comparative study, the three different effects considered in three combinations named as Case I, II and III presented in Table 2. It should be noted that Case II is the geometry of the initial or baseline model. To explore the relationship between the geometrical features on f and j, the flow conditions were simulated with the different heat exchanger models designed based on the dimensions of each case.

Table 2: Cases Considered in the Parametric Study

Geometrical parameter (mm)	Case I	Case II	Case III
F_p	3.7	4.2	4.7
L_p	20	22	24
T_p	23.5	25	26.5

Figure 9 shows a cross-section indicating the longitudinal and transverse pitch geometries respectively. The largest longitudinal and transverse pitch sizes were chosen such that the maximum spacing gives sufficient distance to the edges of the fin. For each L_p and T_p values, the Colburn factor (j) trends were analysed and it characterises the thermal behaviour of the heat exchanger. Finally, the ratio between the two factors (i.e. j/f) known as the efficiency index was also analysed. It should be noted that f and j were calculated using the procedure outlined in section 2.4. Considering each geometrical parameter, a steady-state CFD simulation was performed. The air velocity was varied from 1.0 to 5.0 m/s, while the water velocity was varied from 0.3 to 1.5 m/s. The air inlet temperature was 25 °C while the water inlet temperature was set at 60.0 °C.
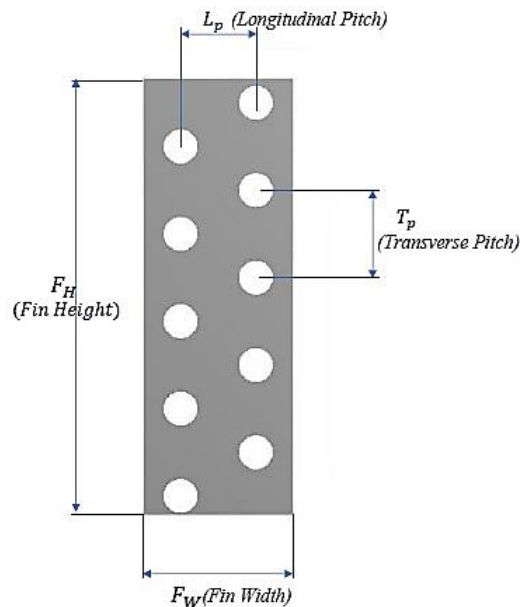

Figure 9: Fin geometry showing longitudinal and transverse pitches

4.3.1 The effect of fin spacing (F_p)

Fin spacing is a key geometrical modification that can affect the performance of a heat exchanger especially on the air side. Studies by Chen and Ren [39] indicate that for a 2-row plate fin and tube heat exchanger, the effect of fin spacing is rather weak. They however noted that this may not be the case when the number of tube and fin rows increase e.g. in multi row tube bundles. This section focuses on the effect of the gaps between fins on the thermal and the pressure drop behaviour of the heat exchanger. The effect limits the number and size of fins that can be mounted along the

tubes in a given space. Results of three fin spacings were investigated i.e. 3.7, 4.2 and 4.7 mm. Shown in Figure 9 are the variations of *j, f,* and *j/f* of the heat exchangers with Re_D for three different fin spacings F_p. Variations of f with Re_D is illustrated in Figure 10 (a). A substantial effect of fin spacing on *f* occurs such that decreasing the fin spacing leads to a decrease in the tube surface area and this clearly affects the pressure drop performance. It was observed that the pressure drop for the 3.7 mm fin spacing case is higher, and this signifies a drawback of small fin spacing despite the increased heat transfer rate obtained. The friction factor value increases by 8.4% and 8.8% when the fin spacing varies within the ranges 4.7–4.2 mm and 4.2–3.7 mm and at Re_D = 18000.
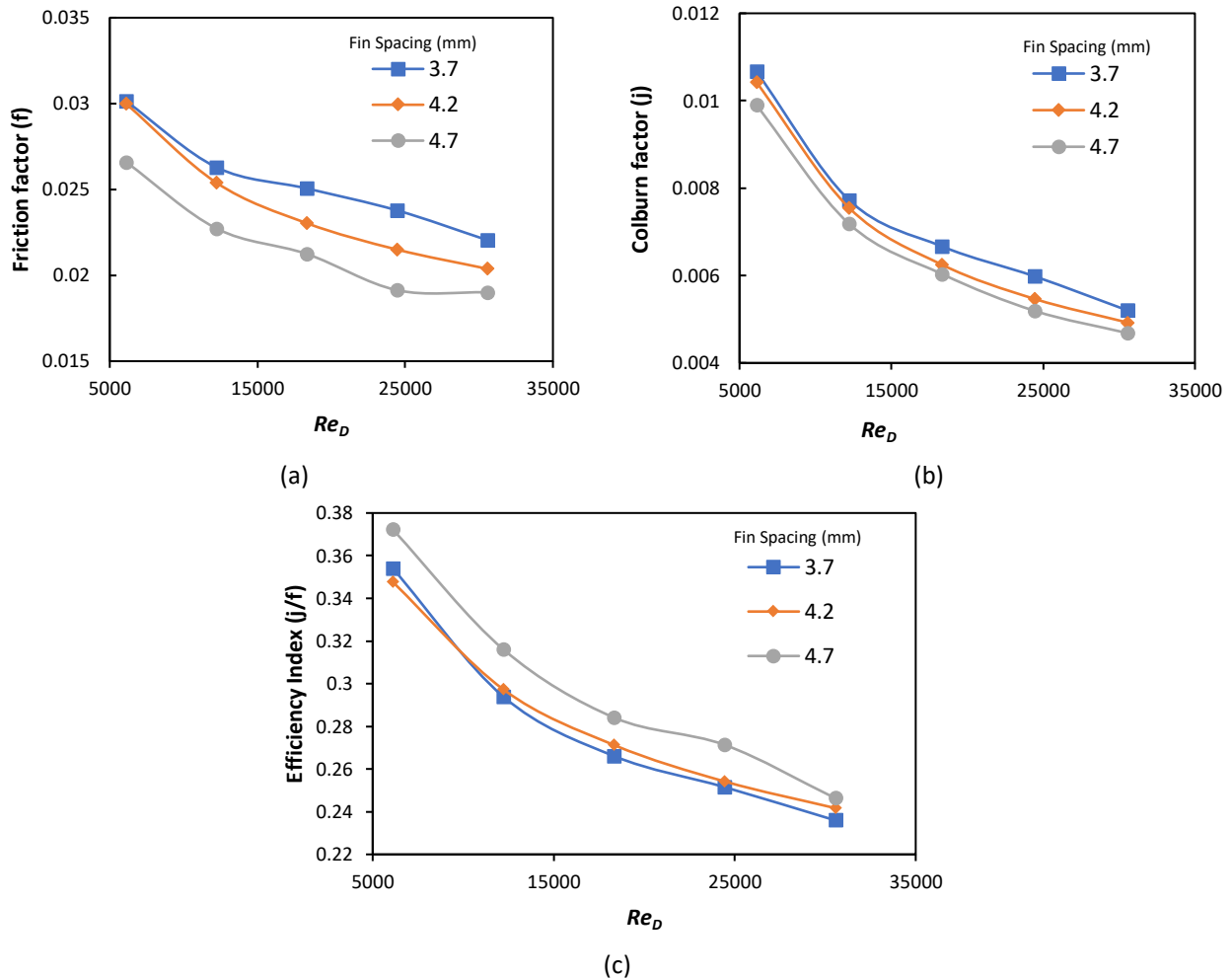

(a)

(b)

(c)

Figure 10: Influence of a variation in fin spacing on the (a) *f* and (b) *j* factor (c) efficiency index

Figure 10 (b) similarly shows that the Colburn factor *j* declines with an increase in the Re. At Re_D = 18000 and when F_p decreases from 4.7 to 4.2 mm. From 4.2 to 3.7 mm, *j* increases by 3.5% and 6.7% respectively. Hence, higher heat transfer occurs for the heat exchanger case having a fin spacing of 3.7 mm. This means that low fin spacing promotes higher heat transfer. It should however be noted that this can come with higher capital costs since more fins are required per unit surface area. Furthermore, it can be said that as F_p decreases, the flow likely becomes more turbulent hence disturbing the development of the turbulent boundary layer. Figure 10 (c) presents variations of *j/f* with Re_D for the three F_p values considered. As before, it shows that *j/f* decreases as Re_D increases with highest value observed to occur at the highest fin spacing of that which was 4.7 mm. The explanation for increased heat transfer with a lower fin spacing value can usually be explained as follows: the boundary layer thickness decreases with fin spacing resulting in an increase in the heat transfer. Nevertheless, this rise has the downside of producing larger pressure drops.

4.3.2   The effect of longitudinal pitch (L_p)

The longitudinal distance or pitch between tubes is important in investigating the heat transfer characteristics of fluid crossflow over heat exchanger tube banks. To examine the effect of arrangement, a widely used approach is to relate the reliance of the heat transfer coefficient [29] on the tube arrangement. Specifically, the magnitude of the longitudinal pitch influences the j factor as well as the f factor. In this section, we assess the effect of the longitudinal pitch size on thermal and pressure drop of the heat exchanger. To evaluate this effect, L_p was varied corresponding to three different configurations of the heat exchanger. These are configurations having L_p = 20 mm, 22 mm, 24 mm. The relationship between the j factor with L_p values are shown in Figure 10. The figure shows that the j factor decreases as L_p increases. For example, j decreases by 10.2% and 3.7% when L_p varies from 20 mm to 24 mm, respectively, for Re_D = 25000. As a result of increasing the surface area of the tube by increasing L_p, the airflow becomes distributed and results in a lower friction factor. Similarly, the same behaviour of f can be seen for j. Such a response contradicts with the phenomenon of increased heat transfer rate with heat transfer area. This is because as L_p decreases the airflow becomes restricted and almost impenetrable due to close tube spacing and this results in an enhancement in heat transfer.
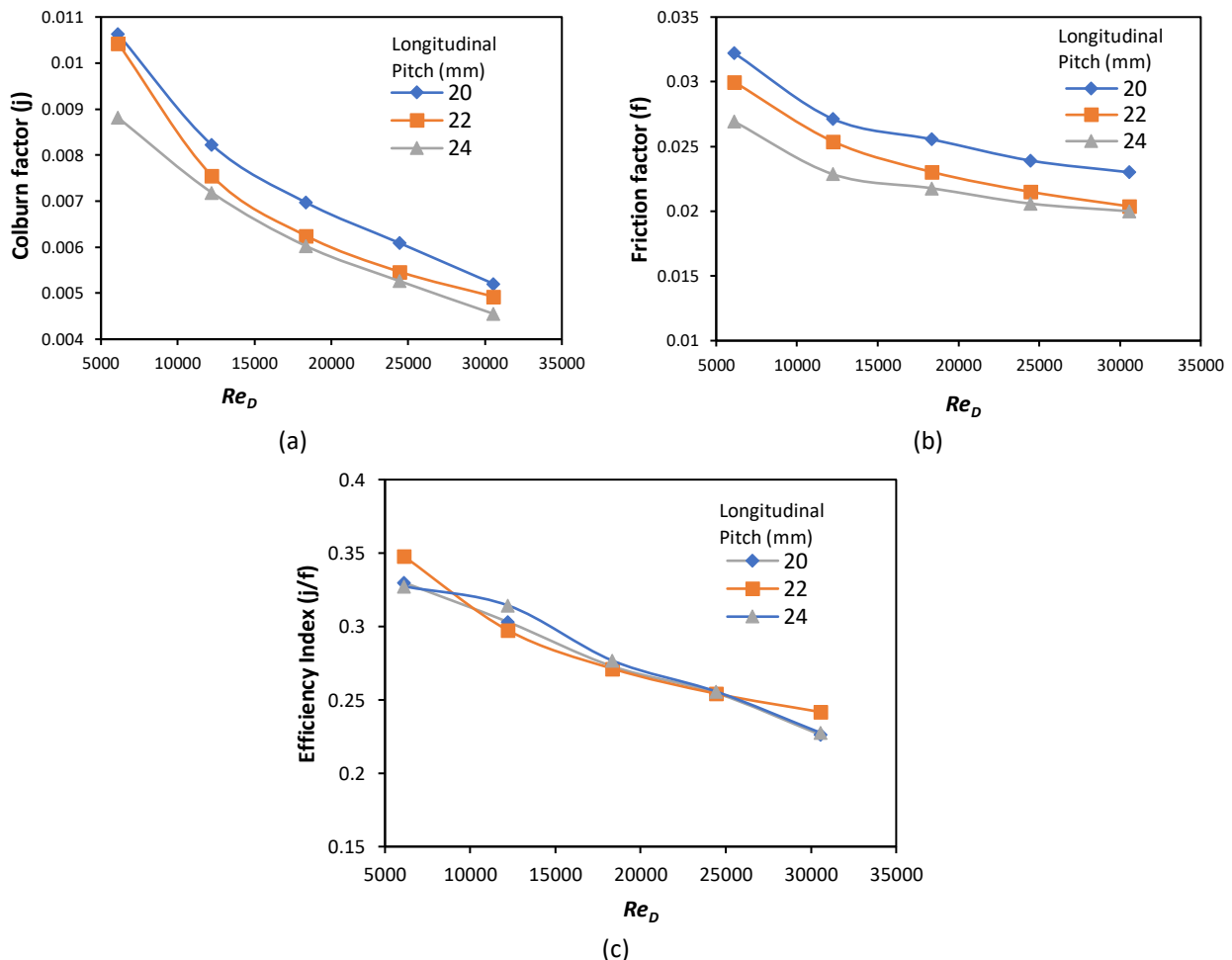

(a)

(b)

(c)

Figure 11: The effect of varying different Lp values on the (a) Colburn factor (b) friction factor (c) efficiency index

Variations of the heat exchangers' Fanning friction factor with Re_D for different L_p values are given in Figure 11 (b). It clearly shows that the friction factor exhibits a similar trend as the Colburn factor as Re_D increases, i.e. an inverse proportionality. Furthermore, a higher magnitude of f occurs at the smallest L_p i.e. 20 mm. In addition, at Re_D = 25000, f decreases by 10.1% and 4.2% when L_p changes from 20 mm to 24 mm respectively. The trends of f and j obtained with Reynolds number

here are similar to those reported by Wang and Chi [6] where they studied the effect of longitudinal pitches (range: 1.22–1.78 mm). While the size of their heat exchanger is smaller than in the current work, it shows increase in *j* and *f* with decreasing pitch. Furthermore, the larger magnitude of *f* over *j* is consistent with the current heat exchanger system indicating pressure drop having a more dominant effect on the flow behaviour over heat transfer characteristics. Figure 11 (c) shows the relationship between the efficiency index with Re_D for the three L_p values studied. It reveals *j/f* decreasing as Re_D increases. Contrary to the trend of *f* and *j*, *j/f* is slightly higher for the larger L_ps at Re_D = 10000–15000. This is because the rate of increase in *j* is lower than that of *f*. However, the changes are very small and could be considered rather insignificant for practical applications.

4.3.3   The effect of Transverse Pitch (T_p)

The transverse pitch is the vertical distance between the heat exchanger tubes and has been identified to play an important role in heat transfer efficiency [40]. In the current section, the influence of transverse pitch on *f* and *j* is investigated. CFD results for three transverse pitches T_p namely 23.5, 25 and 26.5 mm. A comparison will be made to understand transverse pitch effect on the output factors *j*, *f*, and *j/f*. Figure 12 (a) indicates the trend of the heat exchangers *j* factor with Re_D and it shows that the magnitude of T_p clearly affects the Colburn factor which in turn influences the heat transfer rate. In general, *j* decreases as the Re_D increases. At $Re_D = 30000$ and when the T_p is decreases within the two ranges i.e. 26.5 to 25 mm and 25 to 23.5 mm, *j* increases by 7.6% and 3.1%, respectively. Thus, a higher rate of heat transfer occurs for the heat exchanger case having $T_p = 23.5$ mm, i.e. the lowest T_p size considered. This trend exhibited by the heat exchanger is consistent with that exhibited by varying L_p.
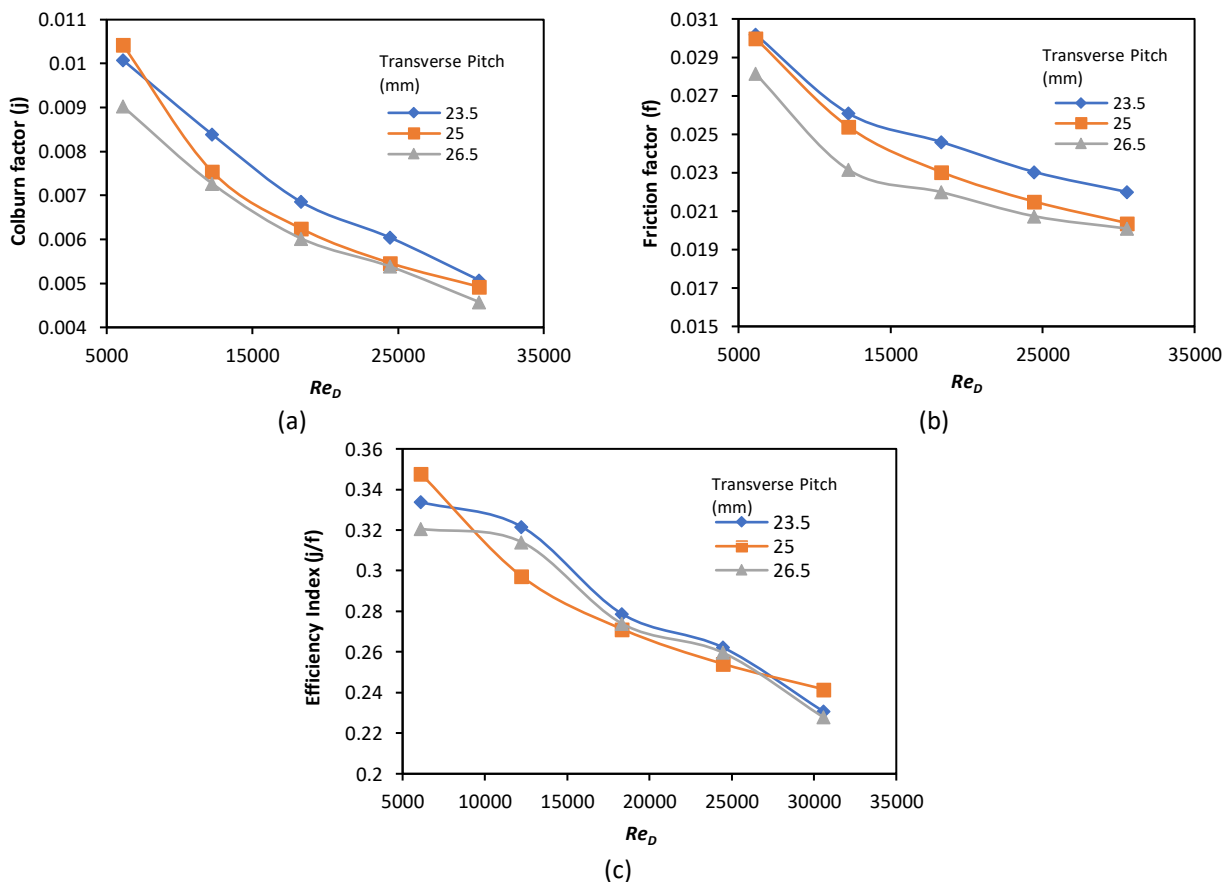

Figure 12: Effect of the Variation of Different Transverse Pitch on (a) Colburn Factor (b) friction factor (c) efficiency index

The variation of f with Re_D for the different T_p values is illustrated in Figure 12 (b). It shows that, as Re_D increases, f tends to decline for all the three cases of T_p. A larger f was obtained at a low T_p of 23.5 mm. Such a trend exhibited by the heat exchanger can be explained by the fact that the surface areas of the tubes increases as T_p increases and an expanding flow area results in lower pressure drop. The variation of j/f with Re_D for each of the T_p values are illustrated in Figure 12 (c). The figure shows that j/f decreases as Re_D increases meaning a higher j/f value occurs at the highest T_p studied i.e. 26.5 mm. This represents a change for the three cases when compared with the behaviour of f and j and this is a reflection of their effect on the thermal and pressure characteristics on the air side.

4.4   New empirical correlations for the Colburn and friction factor

During initial and detailed design stages of process and in particular heat exchanger systems, it is useful to have prior knowledge of the thermal-hydraulic characteristics to enable the determination of desired process variable ranges; selection of process equipment, tube sizes, material types, appropriate material thicknesses, etc. For this reason, the development of empirical correlations relating response parameters such as j and f is of utmost importance. Traditionally, use is made of geometrical features of the heat exchanger as well as its heating and flow parameters to correlate the data in non-dimensional form. For fin-and-tube heat exchangers, previous authors [41], [42] have used the Reynolds number, fin thickness, transverse and longitudinal pitches.

In the current study, the results presented in the previous section which analysed the effect of geometrical features on the thermal performance of the heat exchanger were used to generate a new empirical correlation one for each of f and j factors. As shown, f and j, which represent the pressure drop and thermal characteristics respectively are profoundly affected by the rate of fluid flow and heat exchanger geometry characterised by the fin spacing, as well as their transverse and longitudinal pitch sizes. Therefore, it is imperative to correlate the factors with the geometrical parameters. Hence, the dimensionless quantities used to develop the correlations are Re_D, F_p/D_c, L_p/F_w and T_p/F_H. The application of power law correlation methods with least squares regression is a common approach to related independent variables with output parameters and there are numerous examples of this approach in both open and internal flow research [43]–[45]. The coefficients and indexes of the power law relationships are regression constants that were determined by fitting the CFD data to the power law equation using the least squares method. Applying the method yielded the following relationships for j and f as a function of the fin spacing, longitudinal and transverse pitches, using multiple nonlinear least squares regression as follows:

$$j = 0.047 \, Re_D^{-0.44} \left(F_p / D_c \right)^{-0.41} \left(L_p / F_w \right)^{-0.82} \left(T_p / F_H \right)^{-1.00} \tag{16}$$

$$f = 0.018 \, Re_D^{-0.21} \left(F_p / D_c \right)^{-0.66} \left(L_p / F_w \right)^{-0.88} \left(T_p / F_H \right)^{-0.83} \tag{17}$$

where F_p is the fin spacing, D_c is the outer diameter of the fin collar, F_w is the width of the fin, and F_H is the height of the fin. The form equations are similar in form to those derived by Wang et al. [7] who expressed j and f in terms of the Reynolds number, fin thickness to fin collar outside diameter ratio, dimensionless fin pitch, and number of tube rows for plate fin-and-tube heat exchangers with plane fins. The Reynolds number index was negative as was obtained here indicating an inverse relationship with the j and f factors as shown in Figure 9 to Figure 11. Just as any empirical correlation, Equations (16) and (17) have limitations which include being only applicable to multi-tube and fin heat exchanger with plain fins. They were also developed based on the heating cycle only and do not represent the behaviour of the cooling cycle, and apply to forced convection heat

transfer only. Their application should not be extrapolated far beyond the range of data from which they were derived.
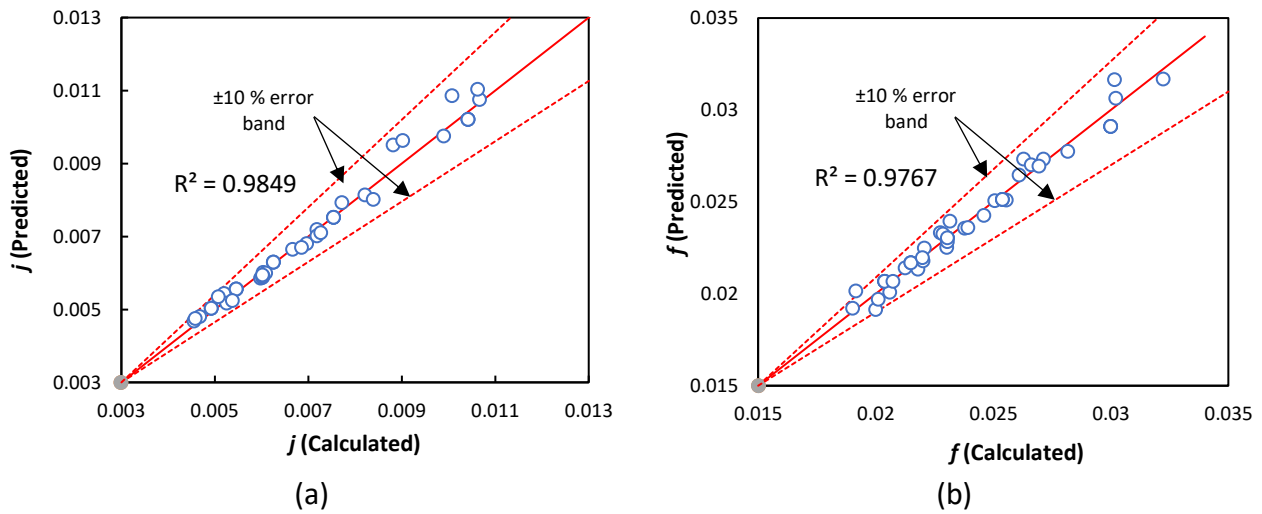

Figure 13: Comparison of the correlation-predicted and CFD-calculated values of the (a) Colburn Factor and (b) Fanning friction factor

The correlation coefficient of the calculated and predicted equation are 0.987 and 0.977, respectively. Based on these, it can be stated that there is a strong correlation between the available data and the developed empirical relationships. As a result, the correlations can be utilised for the design of a multi-tube and fin heat exchanger with plain fins with a significant level of confidence. Figure 13 (a) and (b) shows the relationship between the CFD values and those of j and f predicted by Equations (16) and (17) respectively, and indicates that the percentage changes in the calculated and predicted values of j and f are well within the $\pm$10% error bands. It can therefore be concluded that the correlations can predict the pressure drop and thermal behaviour represented by the f and j factors respectively with satisfactory accuracy.

5   CONCLUSIONS

A detailed well-validated numerical study of the flow characteristics of the working fluids in a multi-tube and fin heat exchanger with plain fins has performed and the main findings of the study can be summarised as follows. A numerical CFD model was created for the full heat exchanger unit, simulated and well-validated against experimental results under a range of operating conditions. It indicated that the CFD model could be used for further investigation including of local parameters with different design modifications. Secondly, the CFD results were used for the determination of heat transfer coefficients, local fin efficiency, and friction factors for the heat exchangers. This analysis shows that full three-dimensional modelling is needed to achieve accurate results. In addition, the results indicate that simplified single-fin geometries often used in literature may not give sufficient accuracy for estimating the thermal and flow performance of the overall FCU. Therefore, simulation using a full 3D CFD model therefore makes an important contribution to the understanding and modelling of such heat exchangers. Under the steady state conditions studied, longitudinal and transverse pitch as well as fin spacing have marked effects on the pressure drop and heat transfer characteristics of the heat exchanger. Minimising the spacing of the fins can improve heat transfer characteristics. Nevertheless, it has the potential to substantially increase the pressure drop across the heat exchanger and hence increased operating costs. Finally, a comprehensive parametric study was done to evaluate the effect of fin spacing, the transverse and longitudinal pitch sizes on the j and f factors of the heat exchanger in several steady state conditions. As a consequence of numerical results of the parametric study, new relationships have been derived for the j and f factors. It was demonstrated that the models can satisfactorily predict

the pressure drop and thermal characteristics as a function of the heat exchanger's geometrical parameters. Both equations can therefore be used dimensional optimisation of a heat exchanger during the design process.

6   NOMENCLATURE

Symbol	Description	Units
A_a	Heat transfer surface areas for air	m^2
A_w	Heat transfer surface areas for water	m^2
A_{wall}	Heat transfer area of the wall	m^2
A_c	Flow cross sectional area	m^2
A_0	Total surface area	m^2
Cp_w	Specific heats for water	J/kg K
Cp_a	Specific heats for air	J/kg K
C_{min}	Mass × Specific heat capacity of fluid with a lower heat capacity rate	kJ/sec K
f	Fanning friction factor	
F_p	Fin spacing	m
f_t	fin thickness	m
h_w	Heat transfer coefficient for water	$W/m^2 K$
h_a	Heat transfer coefficient for air	$W/m^2 K$
j	Colburn factor	
j/f	Efficiency index	
k_{wall}	Thermal conductivity of the wall material	W/m K
K_I	Abrupt contraction pressure-loss coefficient	
K_e	Abrupt expansion pressure-loss coefficient	
K_a	Thermal conductivity of the fin material	W/m K
L_p	Longitudinal pitch	m
$\dot{m}_w$	Mass flow rate for water	kg/sec
$\dot{m}_a$	Mass flow rate for air	kg/sec
Pr	Prandtl number	
ΔP	Pressure drop	Pa
$\dot{Q}_w$	Heat transfer rate for water	W
$\dot{Q}_a$	Heat transfer rate for air	W
$\dot{Q}_{avg}$	Average heat transfer rate	W
R_{wall}	Wall thermal resistance	$m^2 K$
r_o	Outer radius of the tube	m
R	radius of a circular fin which has the same efficiency as the rectangular fin	m
Re_D	Reynolds number	
T_{wi}	Water inlet temperature	K
T_{wo}	Water outlet temperature	K
T_{ai}	Air inlet temperature	K
T_{ao}	Air outlet temperature	K
T_p	Transverse pitch	m
U	Overall heat transfer coefficient	$W/m^2 K$
y^+	Non-dimensional distance from the wall	m

Greek symbols

δ_{wall}	Wall thickness	m
ε	Heat exchanger effectiveness	

η_f	Fin efficiency	%
ρ	Fluid density	kg/m^3
ρ_1	Density of air inlet	kg/m^3
ρ_2	Density of air outlet	kg/m^3
ρ_m	Mean density	kg/m^3
σ	Ratio of the minimum flow area to the frontal area	

CRediT statement

M. Altwieb: Software, data curation, experimentation, analysis, writing – original draft, review and editing. **K. Kubiak:** Writing – review and editing, analysis, supervision. **A. M. Aliyu:** Writing – review and editing. **R. Mishra:** Writing – original draft, review and editing, analysis, supervision.

References

[1]   UK Government, "UK becomes first major economy to pass net zero emissions law," *Gov.uk*, 2019. [Online]. Available: https://www.gov.uk/government/news/uk-becomes-first-major-economy-to-pass-net-zero-emissions-law. [Accessed: 01-May-2020].

[2]   D. Davidson, "Redesign of the Amethyst Fan Coil Unit," University of Huddersfield, 2013.

[3]   A. Cavallini, G. Censi, D. Del Col, L. Doretti, G. A. Longo, and L. Rossetto, "Condensation of halogenated refrigerants inside smooth tubes," *HVAC R Res.*, vol. 8, no. 4, pp. 429–451, 2002.

[4]   S. Mohammadshahi, M. Nili-Ahmadabadi, and O. Nematollahi, "Improvement of ventilation and heat transfer in Shavadoon via numerical simulation: A traditional HVAC system," *Renew. Energy*, vol. 96, pp. 295–304, 2016.

[5]   P. Naphon and S. Wongwises, "A review of flow and heat transfer characteristics in curved tubes," *Renew. Sustain. Energy Rev.*, vol. 10, no. 5, pp. 463–490, Oct. 2006.

[6]   C. C. Wang and K. Y. Chi, "Heat transfer and friction characteristics of plain fin-and-tube heat exchangers, part I: New experimental data," *Int. J. Heat Mass Transf.*, 2000.

[7]   C. C. Wang, Y. J. Chang, Y. C. Hsieh, and Y. T. Lin, "Sensible heat and friction characteristics of plate fin-and-tube heat exchangers having plane fins," *Int. J. Refrig.*, 1996.

[8]   C. C. Wang, Y. P. Chang, K. Y. Chi, and Y. J. Chang, "A study of non-redirection louvre fin-and-tube heat exchangers," *Proc. Inst. Mech. Eng. Part C J. Mech. Eng. Sci.*, vol. 212, no. 1, pp. 1–14, 1998.

[9]   P. Shinde and C. X. Lin, "A heat transfer and friction factor correlation for low air-side Reynolds number applications of compact heat exchangers (1535-RP)," *Sci. Technol. Built Environ.*, vol. 23, no. 1, pp. 192–210, 2017.

[10]   D. Taler, "Experimental and numerical predictions of the heat transfer correlations in the cross-flow plate fin and tube heat exchangers," *Arch. Thermodyn.*, vol. 28, no. 2, pp. 3–18, 2007.

[11]   J. Dong, J. Chen, W. Zhang, and J. Hu, "Experimental and numerical investigation of thermal -hydraulic performance in wavy fin-and-flat tube heat exchangers," *Appl. Therm. Eng.*, vol. 30, no. 11–12, pp. 1377–1386, Aug. 2010.

[12]   C. W. Lu, J. M. Huang, W. C. Nien, and C. C. Wang, "A numerical investigation of the geometric effects on the performance of plate finned-tube heat exchanger," *Energy Convers. Manag.*, 2011.

[13]   Z. M. Lin, L. B. Wang, and Y. H. Zhang, "Numerical study on heat transfer enhancement of circular tube bank fin heat exchanger with interrupted annular groove fin," *Appl. Therm. Eng.*, vol. 73, no. 2, pp. 1465–1476, 2014.

[14]   Z. Čarija, B. Franković, M. Perčić, and M. Čavrak, "Heat transfer analysis of fin-and-tube heat exchangers with flat and louvered fin geometries," *Int. J. Refrig.*, vol. 45, pp. 160–167, Sep. 2014.

[15]   M. O. Altwieb and R. Mishra, "Experimental and Numerical Investigations on the Response of a Multi Tubes and Fins Heat Exchanger under Steady State Operating Conditions Original Citation the Response of a Multi Tubes and Fins Heat Exchanger under," in *6th International and 43rd National Conference on Fluid Mechanics and Fluid Power*, 2016, pp. 1–3.

[16]   C.-C. Wang, K.-Y. Chen, J.-S. Liaw, and C.-Y. Tseng, "An experimental study of the air-side performance of fin-and-tube heat exchangers having plain, louver, and semi-dimple vortex generator configuration," *Int. J. Heat Mass Transf.*, vol. 80, pp. 281–287, Jan. 2015.

[17] ASHRAE, "Standard methods for laboratory air-flow measurement. American Society of Heating, Refrigerating and Air-Conditioning Engineers." Atlanta, p. Standard 41.2-1987, 1987.

[18] E. A. D. Saunders, *Heat Exchangers*. 1988.

[19] K. Thulukkanam, *Heat Exchanger Design Handbook*, 2nd ed. Taylor & Francis, 2013.

[20] R. K. Shah and D. P. Sekulic, *Fundamentals of heat exchanger design*. John Wiley & Sons, 2003.

[21] V. Gnielinski, "New Equations for Heat and Mass Transfer in Turbulent Pipe and Channel Flow," *Int. Chem. Eng.*, vol. 16, no. 2, pp. 359–68, 1976.

[22] W. M. Kays and A. L. London, *Compact heat exchangers*. New York: Hemishphere Publishing, 1984.

[23] Ansys Inc, "ANSYS Fluent User's Guide," 2010.

[24] J. Blazek, *Computational Fluid Dynamics: Principles and Applications*, 3rd ed. Amsterdam: Elsevier, 2015.

[25] A. M. Aliyu, Y. K. Kim, S. H. Choi, J. H. Ahn, and K. C. Kim, "Development of a dual optical fiber probe for the hydrodynamic investigation of a horizontal annular drive gas/liquid ejector," *Flow Meas. Instrum.*, vol. 56, pp. 45–55, Aug. 2017.

[26] J. G. Ardila Marin, D. A. Hincapie Zuluaga, and J. A. Casas Monroy, "Comparison and validation of turbulence models in the numerical study of heat exchangers," *TECCIENCIA*, vol. 10, no. 19, pp. 49–60, Sep. 2015.

[27] H. P. Neopane, *Sediment erosion in hydro turbines*. 2010.

[28] T. J. Craft, "Wall Functions." University of Manchester, Manchester, UK, 2011.

[29] T. Kim, "Effect of longitudinal pitch on convective heat transfer in crossflow over in-line tube banks," *Ann. Nucl. Energy*, vol. 57, pp. 209–215, Jul. 2013.

[30] F. R. Menter, "Two-equation eddy-viscosity turbulence models for engineering applications," *AIAA J.*, vol. 32, no. 8, pp. 1598–1605, Aug. 1994.

[31] R. Mishra, S. N. Singh, and V. Seshadri, "Study of wear characteristics and solid distribution in constant area and erosion-resistant long-radius pipe bends for the flow of multisized particulate slurries," *Wear*, vol. 217, no. 2, pp. 297–306, May 1998.

[32] Y. Xue, Z. Ge, X. Du, and L. Yang, "On the Heat Transfer Enhancement of Plate Fin Heat Exchanger," *Energies*, vol. 11, no. 6, p. 1398, May 2018.

[33] M. R. Shaeri, M. Yaghoubi, and K. Jafarpur, "Heat transfer analysis of lateral perforated fin heat sinks," *Appl. Energy*, vol. 86, no. 10, pp. 2019–2029, Oct. 2009.

[34] A. H. AlEssa, A. M. Maqableh, and S. Ammourah, "Enhancement of natural convection heat transfer from a fin by rectangular perforations with aspect ratio of two," *Int. J. Phys. Sci.*, vol. 4, no. 10, pp. 540–547, 2009.

[35] R. A. Schwentker, "Advances to a computer model used in the simulation and optimization of heat exchangers.," University of Maryland.

[36] T. E. Schmidt, "Heat transfer calculations for extended surfaces," *Refrig. Eng.*, vol. 57, no. 4, pp. 351–357, 1949.

[37] F. C. Mcquiston, J. D. Parker, and J. K. Spilter, *Heating, ventilating, and air conditioning: analysis and design*. Wiley, 2004.

[38] R. K. Shah and A. L. London, *Laminar flow forced convection in ducts: a source book for compact heat exchanger analytical data*. Adademic Press, 2014.

[39] Z. Q. Chen and J. X. Ren, "Effect of fin spacing on the heat transfer and pressure drop of a two-row plate fin and tube heat exchanger," *Int. J. Refrig.*, vol. 11, no. 6, pp. 356–360, Nov. 1988.

[40] K. Sahim, "Effect of transverse pitch on forced convective heat transfer over single row cylinder," *Int. J. Mech. Mater. Eng.*, vol. 10, no. 1, p. 16, Dec. 2015.

[41] D. E. Briggs and E. H. Young, "Convection Heat Transfer and Pressure Drop of Air Flowing across Triangular Pitch Banks of Finned Tubes," *Chem. Eng. Prog. Symp. Ser.*, vol. 59, no. 41, pp. 1–10, 1963.

[42] T. J. Rabas, P. W. Eckels, and R. A. Sabatino, "The effect of fin density on the heat transfer and pressure drop performance of low-finned tube banks," *Chem. Eng. Commun.*, vol. 10, no. 1–3, pp. 127–147, Jan. 1981.

[43] A. M. Aliyu, H. Seo, M. Kim, and K. C. Kim, "An experimental study on the characteristics of ejector-generated bubble swarms," *J. Vis.*, pp. 1–18, May 2018.

[44] Y. D. Baba, A. M. Aliyu, A.-E. Archibong, A. A. Almabrok, and A. I. Igbafe, "Study of high viscous multiphase phase flow in a horizontal pipe," *Heat Mass Transf.*, Sep. 2017.

[45] A. M. Aliyu, H. Seo, H. Kim, and K. C. Kim, "Characteristics of bubble-induced liquid flows in a rectangular tank," *Exp. Therm. Fluid Sci.*, vol. 97, no. March, pp. 21–35, 2018.